

# Fundamental Understanding of Piezoelectric Strain Sensors

JAYANT SIROHI\* AND INDERJIT CHOPRA

*Alfred Gessow Rotorcraft Center, Department of Aerospace Engineering, University of Maryland, College Park, MD 20742*

**ABSTRACT:** This paper investigates the behavior of piezoelectric elements as strain sensors. Strain is measured in terms of the charge generated by the element as a result of the direct piezoelectric effect. Strain measurements from piezoceramic (PZT) and piezofilm (PVDF) sensors are compared with strains from a conventional foil strain gage and the advantages of each type of sensor are discussed, along with their limitations. The sensors are surface bonded to a beam and are calibrated over a frequency range of 5–500 Hz. Correction factors to account for transverse strain and shear lag effects due to the bond layer are analytically derived and experimentally validated. The effect of temperature on the output of PZT strain sensors is investigated. Additionally, design of signal conditioning electronics to collect the signals from the piezoelectric sensors is addressed. The superior performance of piezoelectric sensors compared to conventional strain gages in terms of sensitivity and signal to noise ratio is demonstrated.

## INTRODUCTION

PIEZOELECTRIC elements are commonly used in smart structural systems as both sensors and actuators (Chopra, 1996). A key characteristic of these materials is the utilization of the converse piezoelectric effect to actuate the structure in addition to the direct effect to sense structural deformation. Typically, piezoceramics are used as actuators and polymer piezo films are used as sensing materials. It is also possible to use piezoceramics for both sensing and actuation, as in the case of self-sensing actuators (Inman et al., 1992). In addition to the possibility of performing collocated control, such actuators/sensors have other advantages such as compactness, sensitivity over a large strain bandwidth and ease of embeddability for performing structural health monitoring as well as distributed active control functions concurrently. Many researchers have used piezoceramic sheet elements as sensors in controllable structural systems (Qui and Tani, 1995) and also in health monitoring applications (Samuel and Pines, 1997). Most of these applications rely on the relative magnitudes of either the voltage or rate of change of voltage generated by the sensor, or the frequency spectrum of the signal generated by the sensor. Several investigations have been carried out on discrete piezoelectric sensor systems (Qui and Tani, 1995), active control of structures with feedback from piezoelectric sensors (Hanagud et al., 1992), and collocated sensors and actuators (Inman et al., 1992; Anderson and Hagood, 1994). However, a limited attempt has been made to accurately calibrate the magnitude of the measured sensor voltage with actual structural strain.

Piezoelectric strain rate sensors have been investigated by Lee and O'Sullivan (1991) and Lee et al. (1991) wherein

their superior noise immunity as compared to differentiated signals from conventional foil gages has been demonstrated. The correlation between the piezoelectric gage reading and the foil gage measurement is quite good; however the comparison was performed only at one frequency, 25 Hz.

The work presented in this paper is an attempt to calibrate piezoelectric strain sensors by comparing their calculated strain output to a conventional foil strain gage measurement. Appropriate signal conditioning electronics is developed to collect the data from the strain sensor. The transfer functions of both types of sensors are compared over a frequency range from 5–500 Hz.

## PIEZOELECTRIC SENSORS

### Constitutive Relations

Under small field conditions, the constitutive relations for a piezoelectric material are (IEEE Standard, 1987):

$$D_i = e_{ij}^{\sigma} E_j + d_{im}^d \sigma_m \quad (1)$$

$$\epsilon_k = d_{jk}^c E_j + s_{km}^E \sigma_m \quad (2)$$

which can be rewritten as

$$\begin{bmatrix} \mathbf{D} \\ \boldsymbol{\epsilon} \end{bmatrix} = \begin{bmatrix} \mathbf{e}^{\sigma} & \mathbf{d}^d \\ \mathbf{d}^c & \mathbf{s}^E \end{bmatrix} \begin{bmatrix} \mathbf{E} \\ \boldsymbol{\sigma} \end{bmatrix} \quad (3)$$

where vector  $\mathbf{D}$  of size  $(3 \times 1)$  is the electric displacement (Coulomb/m<sup>2</sup>),  $\boldsymbol{\epsilon}$  is the strain vector  $(6 \times 1)$  (dimensionless),  $\mathbf{E}$  is the applied electric field vector  $(3 \times 1)$  (Volt/m) and  $\boldsymbol{\sigma}_m$  is the stress vector  $(6 \times 1)$  (N/m<sup>2</sup>). The piezoelectric constants

\*Author to whom correspondence should be addressed. E-mail: [sirohij@eng.umd.edu](mailto:sirohij@eng.umd.edu)

are the dielectric permittivity  $e_{ij}^\sigma$  of size  $(3 \times 3)$  (Farad/m), the piezoelectric coefficients  $d_{im}^d$  ( $3 \times 6$ ) and  $d_{jk}^c$  ( $6 \times 3$ ) (Coulomb/N or m/Volt), and the elastic compliance  $s_{km}^E$  of size  $(6 \times 6)$  ( $\text{m}^2/\text{N}$ ). The piezoelectric coefficient  $d_{jk}^c$  (m/Volt) defines strain per unit field at constant stress and  $d_{im}^d$  (Coulomb/N) defines electric displacement per unit stress at constant electric field. The superscripts  $c$  and  $d$  have been added to differentiate between the converse and direct piezoelectric effects, though in practice, these coefficients are numerically equal. The superscripts  $\sigma$  and  $E$  indicate that the quantity is measured at constant stress and constant electric field respectively. For a sheet of piezoelectric material, the poling direction which is usually along the thickness, is denoted as the 3-axis and the 1-axis and 2-axis are in the plane of the sheet. The  $d_{jk}^c$  matrix can then be expressed as

$$\mathbf{d} = \begin{bmatrix} 0 & 0 & d_{31} \\ 0 & 0 & d_{32} \\ 0 & 0 & d_{33} \\ 0 & d_{24} & 0 \\ d_{15} & 0 & 0 \\ 0 & 0 & 0 \end{bmatrix} \quad (4)$$

where the coefficients  $d_{31}$ ,  $d_{32}$  and  $d_{33}$  relate the normal strain in the 1, 2 and 3 directions respectively to a field along the poling direction,  $E_3$ . The coefficients  $d_{15}$  and  $d_{24}$  relate the shear strain in the 1-3 plane to the field  $E_1$  and shear strain in the 2-3 plane to the  $E_2$  field, respectively. Note that it is not possible to obtain shear in the 1-2 plane purely by application of an electric field.

In general, the compliance matrix is of the form

$$\mathbf{s}^E = \begin{bmatrix} S_{11} & S_{12} & S_{13} & 0 & 0 & 0 \\ S_{12} & S_{22} & S_{23} & 0 & 0 & 0 \\ S_{13} & S_{23} & S_{33} & 0 & 0 & 0 \\ 0 & 0 & 0 & S_{44} & 0 & 0 \\ 0 & 0 & 0 & 0 & S_{55} & 0 \\ 0 & 0 & 0 & 0 & 0 & S_{66} \end{bmatrix} \quad (5)$$

and the permittivity matrix is

$$\mathbf{e}^\sigma = \begin{bmatrix} e_{11}^\sigma & 0 & 0 \\ 0 & e_{22}^\sigma & 0 \\ 0 & 0 & e_{33}^\sigma \end{bmatrix} \quad (6)$$

The stress vector is written as

$$\boldsymbol{\sigma} = \begin{bmatrix} \sigma_1 \\ \sigma_2 \\ \sigma_3 \\ \sigma_4 \\ \sigma_5 \\ \sigma_6 \end{bmatrix} = \begin{bmatrix} \sigma_{11} \\ \sigma_{22} \\ \sigma_{33} \\ \sigma_{23} \\ \sigma_{31} \\ \sigma_{12} \end{bmatrix} \quad (7)$$

Equation (1) is the sensor equation and Equation (2) is the actuator equation. Actuator applications are based on the converse piezoelectric effect. The actuator is bonded to a structure and an external electric field is applied to it, which results in an induced strain field. Sensor applications are based on the direct effect. The sensor is exposed to a stress field, and generates a charge in response, which is measured. In the case of a sensor, where the applied external electric field is zero, Equation (3) becomes

$$\begin{bmatrix} D_1 \\ D_2 \\ D_3 \end{bmatrix} = \begin{bmatrix} 0 & 0 & 0 & 0 & d_{15} & 0 \\ 0 & 0 & 0 & d_{24} & 0 & 0 \\ d_{31} & d_{32} & d_{33} & 0 & 0 & 0 \end{bmatrix} \begin{bmatrix} \sigma_1 \\ \sigma_2 \\ \sigma_3 \\ \sigma_4 \\ \sigma_5 \\ \sigma_6 \end{bmatrix} \quad (8)$$

This equation summarizes the principle of operation of piezoelectric sensors. A stress field causes an electric displacement to be generated [Equation (8)] as a result of the direct piezoelectric effect. Note that shear stress in the 1-2 plane,  $\sigma_6$  is not capable of generating any electric response.

The electric displacement  $D$  is related to the generated charge by the relation

$$q = \iint [D_1 \quad D_2 \quad D_3] \begin{bmatrix} dA_1 \\ dA_2 \\ dA_3 \end{bmatrix} \quad (9)$$

where  $dA_1$ ,  $dA_2$  and  $dA_3$  are the components of the electrode area in the 2-3, 1-3 and 1-2 planes respectively. It can be seen that the charge collected,  $q$ , depends only on the component of the infinitesimal electrode area  $d\mathbf{A}$  normal to the displacement  $\mathbf{D}$ . The charge  $q$  and the voltage generated across the sensor electrodes  $V_c$  are related by the capacitance of the sensor,  $C_p$  as

$$V_c = q / C_p \quad (10)$$

Therefore, by measuring the charge generated by the piezoelectric material, from Equations (8) and (9), it is possible to calculate the stress in the material. From these values, knowing the compliance of the material, the strain in the material is calculated.

The sensors used in this work are all in the form of sheets (Figure 1), with its two faces coated with thin electrode layers. The 1 and 2 axes of the piezoelectric material are in the plane of the sheet. In the case of a uniaxial stress field, the correlation between strain and charge developed is simple. However, for the case of a general plane stress distribution in the 1-2 plane, this correlation is complicated by the presence of the  $d_{32}$  term in the  $\mathbf{d}^d$  matrix.

While any piezoelectric material can be used as a sensor, the present study is focused to two types of piezoelectric materials, and they are piezoceramics and polymer piezoelectric

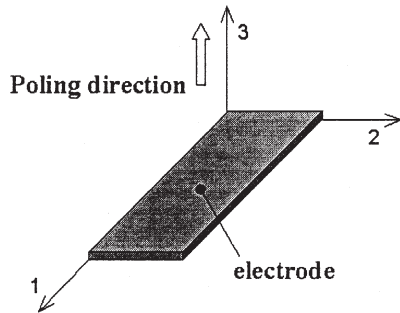


Figure 1. Piezoelectric sheet.

film. The characteristics of each type of material are discussed below.

### PZT Sensors

The most commonly used type of piezoceramics, Lead Zirconate Titanates (PZTs) are solid solutions of lead zirconate and lead titanate, often doped with other elements to obtain specific properties. These ceramics are manufactured by mixing together proportional amounts of lead, zirconium and titanium oxide powders and heating the mixture to around 800–1000°C. They then react to form the perovskite PZT powder. This powder is mixed with a binder and sintered into the desired shape. During the cooling process, the material undergoes a paraelectric to ferroelectric phase transition and the cubic unit cell becomes tetragonal. As a result, the unit cell becomes elongated in one direction and has a permanent dipole moment oriented along its long axis (*c*-axis). The unpoled ceramic consists of many randomly oriented domains and thus has no net polarization. Application of a high electric field has the effect of aligning most of the unit cells as closely parallel to the applied field as possible. This process is called poling and it imparts a permanent net polarization to the ceramic. The material in this state exhibits both the direct and converse piezoelectric effects.

PZT sensors exhibit most of the characteristics of ceramics, namely a high elastic modulus, brittleness and low tensile strength. The material itself is mechanically isotropic, and by virtue of the poling process, is assumed transversely isotropic in the plane normal to the poling direction as far as piezoelectric properties are concerned. This means that for PZT sensors,  $s_{11} = s_{22}$ ,  $s_{13} = s_{23}$ ,  $s_{44} = s_{55}$ ,  $d_{31} = d_{32}$  and  $d_{15} = d_{24}$ .

### PVDF Sensors

PVDF is a polymer (Polyvinylidene Fluoride), consisting of long chains of the repeating monomer ( $-\text{CH}_2-\text{CF}_2-$ ). The hydrogen atoms are positively charged and the fluorine atoms are negatively charged with respect to the carbon atoms and this leaves each monomer unit with an inherent dipole moment. PVDF film is manufactured by solidification of the film from a molten phase, which is then stretched in a

Table 1. Typical properties at 25°C.

	PZT-5H	PVDF
Young's modulus (GPa)	71	4–6
$d_{31}$ (pC/N)	-274	18–24
$d_{32}$ (pC/N)	-274	2.5–3
$d_{33}$ (pC/N)	593	-33
$e_{33}$ (nC/m)	30.1	0.106

particular direction and finally poled. In the liquid phase, the individual polymer chains are free to take up any orientation and so a given volume of liquid has no net dipole moment. After solidification, and stretching the film in one direction, the polymer chains are mostly aligned along the direction of stretching. This, combined with the poling, imparts a permanent dipole moment to the film, which then behaves like a piezoelectric material.

The process of stretching the film, which orients the polymer chains in a specific direction, renders the material piezoelectrically orthotropic, which means  $d_{31} \neq d_{32}$ . The stretching direction is taken as the 1-direction. For small strains, however, the material is considered mechanically isotropic.

The typical characteristics of PZT and PVDF are compared in Table 1. The Young's modulus of the PZT material is comparable to that of aluminum, whereas that of PVDF is approximately 1/12th that of aluminum. It is therefore much more suited to sensing applications since it is less likely to influence the dynamics of the host structure as a result of its own stiffness. It is also very easy to shape PVDF film for any desired application. These characteristics make PVDF films more attractive for sensor applications compared to PZT sensors, in spite of their lower piezoelectric coefficients (approximately 1/10th of PZT). Also, PVDF is pyroelectric, and this translates to a highly temperature dependent performance compared to PZT sensors.

## SENSOR CALIBRATION

### Experimental Setup

A dynamic beam bending setup was used to calibrate the piezoelectric sensors. A pair of PZT sheets is bonded 20 mm from the root of a cantilevered aluminum beam of dimensions 280 × 11 × 1.52 mm, and connected so as to provide a pure bending actuation to the beam. A conventional foil type strain gage is bonded on the beam surface at a location approximately 50 mm from the end of the actuators, and a piezoelectric sensor is bonded at the same location on the other face of the beam so that both sensors are exposed to the same strain field. A sketch of the experimental setup is shown in Figure 2. The strain reading from the foil gage is recorded using a conventional signal conditioning unit and the strain is

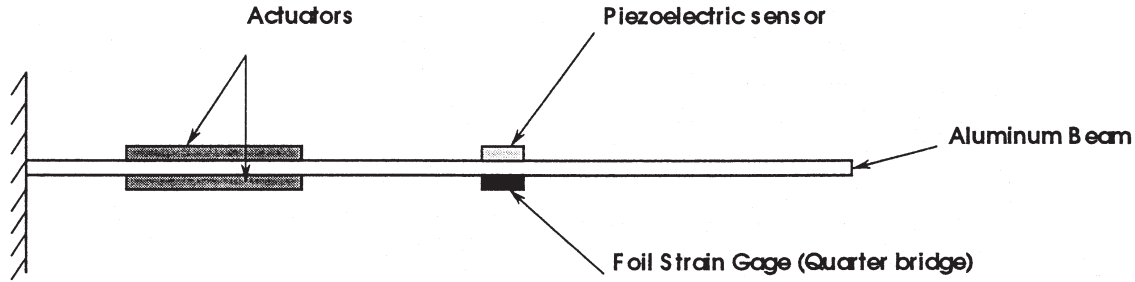


Figure 2. Calibration setup.

calculated using standard calibration formulae. The output of the piezoelectric sensor is measured using conditioning electronics and converted to strain. A sine sweep is performed from 5–500 Hz and the transfer functions of the two sensors are compared.

### Conversion of Voltage Output to Strain

A typical piezoelectric sheet can be treated as a parallel plate capacitor, whose capacitance is given by

$$C_p = \frac{e_{33}^S l_c b_c}{t_c} \quad (11)$$

where  $l_c$ ,  $b_c$  and  $t_c$  are length, width, and thickness of the sensor respectively. The relation between charge stored and voltage generated across the electrodes of the capacitor is given by Equation (10). Considering only the effect of strain along the 1-direction, from Equations (8), (9), (10) and (11) the voltage generated by the sensor can be expressed as

$$V_c = \frac{d_{31} Y_c b_c}{C_p} \int_{l_c} \epsilon_1 dx \quad (12)$$

Assuming the value of  $\epsilon_1$  to be averaged over the gage length, and defining a sensitivity parameter

$$S_q = d_{31} Y_c l_c b_c \quad (13)$$

where  $Y_c$  is the Young's modulus of the piezoelectric material. The equation relating strain and voltage generated by the sensor is

$$\epsilon_1 = \frac{V_c C_p}{S_q} \quad (14)$$

The measurement of the voltage  $V_c$  is discussed below.

### Signal Conditioning

The output of the piezoelectric sensor has to be passed through some signal conditioning electronics in order to accurately measure the voltage being developed by the sensor.

This is because the piezoelectric sensor typically has a very high output impedance, while the measuring device, a voltmeter for example, has an input impedance on the order of several  $M\Omega$ , which is much lower than the output impedance of the sensor. Most oscilloscopes and data acquisition systems have an input impedance of 1  $M\Omega$ . The primary purpose of the signal conditioning system is to provide a signal with a low output impedance while simultaneously presenting a very high input impedance to the piezoelectric sensor. There are several ways of achieving this (Dally et al., 1993; Stout, 1976). One way is to short the electrodes of the sensor with an appropriate resistance and measure the current flowing through the resistance by means of a voltage follower. Since current is the rate of change of charge, measuring the current flowing through the sensor is equivalent to measuring the strain rate directly. This method was investigated by Lee and O'Sullivan (1991) and Lee et al. (1991), wherein the current is measured by means of a current amplifier. The procedure followed in the present work is to make use of a charge amplifier to measure the charge generated by the sensor, which is equivalent to measuring its strain.

The signal conditioning circuit used in this investigation is shown in Figure 3. The piezoelectric sensor can be modeled as a charge generator in parallel with a capacitance,  $C_p$ , equal to the capacitance of the sensor. The cables which carry the signal to the charge amplifier, collectively act as a capacitance  $C_c$  in parallel with the sensor. The charge amplifier has several advantages (Dally et al., 1993). First, as will be

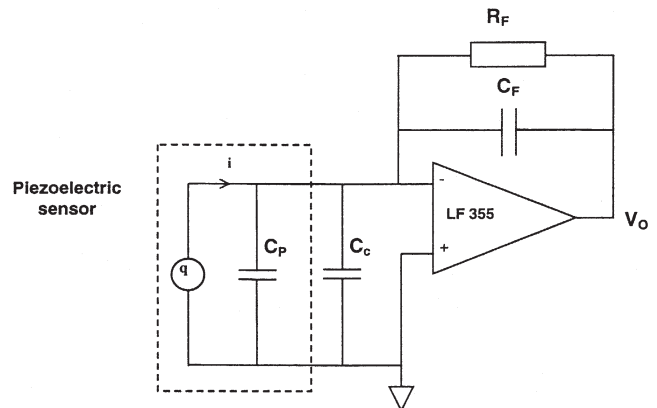
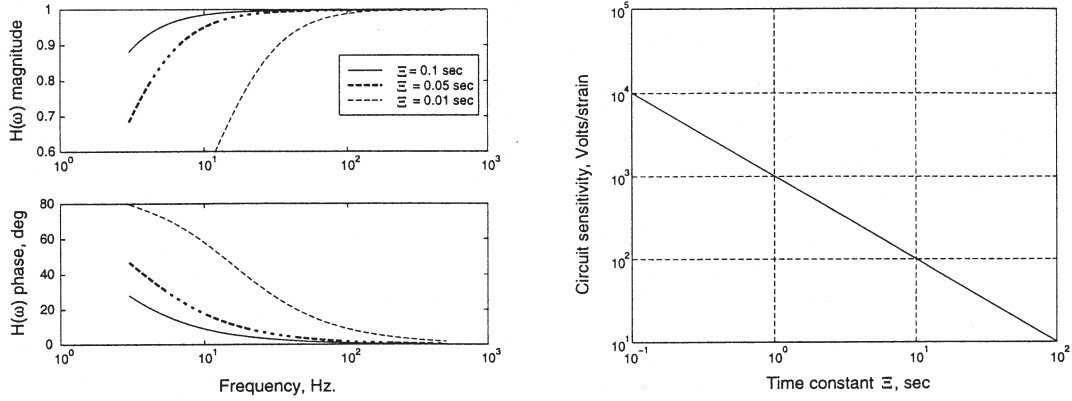


Figure 3. Charge amplifier circuit.



(a) Circuit transfer function, for different time constants (b) Tradeoff between sensitivity and time constant

Figure 4. Circuit characteristics.

shown below, the charge generated by the sensor is transferred onto the feedback capacitance,  $C_F$ . This means that once the value of  $C_F$  is known and fixed, the calibration factor is fixed, irrespective of the capacitance of the sensor. Second, the value of the time constant, which is given by  $R_F C_F$  can be selected to give the required dynamic frequency range. It is to be noted, however, that there is always some finite leakage resistance in the piezoelectric material, which causes the generated charge to leak off. Therefore, though the time constant of the circuit can be made very large to enable operation at very low frequencies, it is not possible to determine a pure static condition. This basic physical limitation exists for all kinds of sensors utilizing the piezoelectric effect. Third, the effect of the lead wire capacitance,  $C_c$ , which is always present for any physical measurement system, is eliminated. This has the important consequence that there are no errors introduced in the measurements by the lead wires.

Considering only the charge generated by strain in the 1-direction, the current  $i$  can be expressed as

$$i = \dot{q} = d_{31} Y_c l_c b_c \dot{\epsilon}_1 \quad (15)$$

$$= S_q \dot{\epsilon}_1 \quad (16)$$

Assuming ideal operational amplifier characteristics, the governing differential equation of the circuit can be derived to be

$$\dot{V}_0 + \frac{V_0}{R_F C_F} = -\frac{S_q \dot{\epsilon}_1}{C_F} \quad (17)$$

which, for harmonic excitation, has the solution

$$\bar{V}_0 = -\left( \frac{j\omega R_F C_F}{1 + j\omega R_F C_F} \right) \frac{S_q \bar{\epsilon}_1}{C_F} \quad (18)$$

$$= H(\omega) (-S_q^* \bar{\epsilon}_1) \quad (19)$$

where the quantities with a bar represent their magnitudes, and  $\omega$  is the frequency of operation. The quantity  $S_q^*$  is called the circuit sensitivity, representing the output voltage per unit strain input, and is given by

$$S_q^* = \frac{d_{31} Y_c l_c b_c}{C_F} \quad (20)$$

The magnitude and phase of the gain  $H(\omega)$  are plotted in Figure 4(a) for different values of time constant, while keeping  $R_F = 10 \text{ M}\Omega$ . It can be seen that this represents a high pass filter characteristic, with a time constant  $\Theta = R_F C_F$ . As discussed before, the value of this time constant can be made very large for low frequency measurements. Another point to be noted is that the sensitivity of the circuit depends inversely on the value of the feedback capacitance,  $C_F$ . For a given strain, as the value of  $C_F$  decreases, the output voltage  $V_0$  will increase. However, this capacitance cannot be decreased indefinitely. From Equation (18), it can be seen that the lower cutoff frequency of the circuit varies directly with  $C_F$ . This tradeoff is shown in Figure 4(b), assuming a fixed value of  $R_F$  of  $10 \text{ M}\Omega$ . Though larger time constants are possible with larger values of feedback resistance, it is not practical to increase the value of the feedback resistor  $R_F$  beyond the order of tens of megaohms due to various operational constraints. For a time constant of the order of 0.1 seconds, the circuit sensitivity is of the order of  $10^4$  volts/strain, which translates to an output voltage in the millivolt range in response to a one microstrain input. This sensitivity is achievable in a conventional foil strain gage only after extensive amplification and signal conditioning is incorporated. It can be seen that for larger time constants, the sensitivity drops, which means that as a pure static condition is approached, the output signal becomes weaker. Hence, as discussed before, it is not possible to measure pure static or quasi-static conditions. The major advantage of the charge amplifier comes from the fact that the circuit sensitivity, and therefore, the output voltage is unaffected by the capacitance of the sensor and stray capacitances like the input cable capacitance. The output depends

only on the feedback capacitor. This makes it easy to use the same circuit with different sensors without changing the calibration factor.

### Correction Factors

It is to be noted that the derivation of Equation (14) was based on the assumption that only strain in the 1-direction contributed to the charge generated, the effect of other strain components was negligible, and that there is no loss of strain in the bond layer. In reality however, a transverse component of strain exists and there are some losses in the finite thickness bond layer. Hence, the value of strain as calculated by this equation is not the actual strain which is measured by the strain gage. Several correction factors are required to account for transverse strain and shear lag losses in the bond layer. These correction factors are discussed below.

### Poisson's Ratio Effect

The sensor on the beam is in reality exposed to both longitudinal and transverse strains. If the 1-direction is assumed to coincide with the length dimension of the beam and the 2-direction with the width direction of the beam, Equation (8) can be rewritten as

$$D = d_{31}Y_{11}\varepsilon_1 + d_{32}Y_{22}\varepsilon_2 \quad (21)$$

For a longitudinal stress, there will be a lateral strain due to Poisson's effect at the location of the sensor,

$$\varepsilon_2 = -\nu\varepsilon_1 \quad (22)$$

where  $\nu$  is the Poisson's ratio of the host structure material, which in this case, is aluminum ( $\nu = 0.3$ ). Hence, Equation (14) can be rewritten as

$$\varepsilon_1 = \frac{V_o}{K_p S_q^*} \quad (23)$$

where  $K_p$  is the correction factor due to Poisson's effect. For PZT sensors, it can be seen that

$$K_p = (1 - \nu) \quad (24)$$

for PVDF sensors,  $K_p$  is given by

$$K_p = \left(1 - \nu \frac{d_{32}}{d_{31}}\right) \quad (25)$$

This is a key distinction between piezoelectric sensors and conventional foil gages. The transverse sensitivity of a piezoelectric sensor is of the same order as its longitudinal sensitivity. However, for a conventional strain gage, the transverse sensitivity is close to zero and is normally neglected. Hence, in a general situation, it is not possible to separate out the principal strains of a structure using only one piezoelectric sensor. At least two sensors are required, constructed out of a piezoelectrically or mechanically orthotropic material. Therefore, this rules out the use of PZT sensors where both longitudinal and transverse strain measurements are required. For calibration, the transverse strain is known a priori, which enables the derivation of a correction factor.

### Shear Lag Effect

The derivation of the correction factor to account for shear lag effects caused by a finite thickness bond layer proceeds along the lines of that presented by Crawley and de Luis (1987). Consider a sensor of length  $l_c$ , width  $b_c$ , thickness  $t_c$  and Young's modulus  $Y_c$  bonded onto the surface of a beam of length  $l_b$ , width  $b_b$ , thickness  $t_b$  and Young's modulus  $Y_b$ . Let the thickness of the bond layer be  $t_s$  (Esteban et al., 1996; Lin and Rogers, 1993, 1994). Assuming the beam to be actuated in pure bending, the forces and moments acting on the beam can be represented as shown in Figure 5. Linear strain distribution across the thickness of the beam is assumed, and the actuator thickness is considered small compared to the beam thickness. The strain is assumed constant across the thickness of the actuator. Force equilibrium in the sensor along the  $x$  direction gives

$$\frac{\partial \sigma_c}{\partial x} t_c - \tau = 0 \quad (26)$$

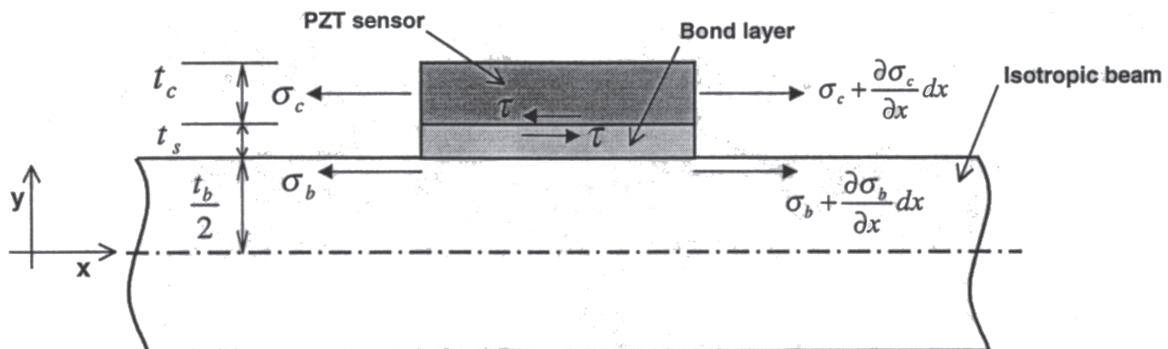


Figure 5. Forces and moments acting on the sensor.

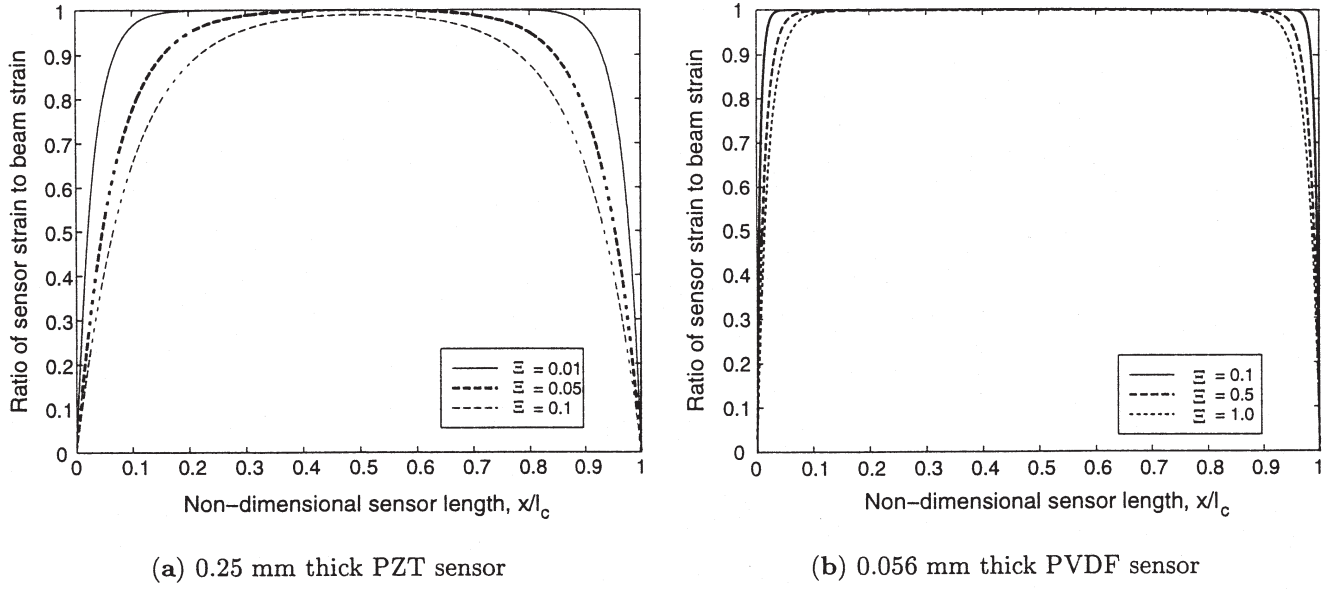


Figure 6. Shear lag effects along sensor length.

and moment equilibrium in the beam gives

$$\frac{\partial \sigma_b}{\partial x} + \tau \frac{3b_c}{b_b t_b} = 0 \quad (27)$$

The strains can be related to the displacements by

$$\varepsilon_c = \frac{\partial u_c}{\partial x} \quad (28)$$

$$\varepsilon_b = \frac{\partial u_b}{\partial x} \quad (29)$$

$$\gamma = \frac{1}{t_s} (u_c - u_b) \quad (30)$$

where  $u_c$  and  $u_b$  are the displacements of the sensor and on the beam surface respectively, and  $\gamma$  is the shear strain in the bond layer.

Substituting Equations (28–30) in Equations (26) and (27), and simplifying leads to the relation

$$\frac{\partial^2 \zeta}{\partial x^2} - \left[ \frac{G}{Y_c t_c t_s} + \frac{3b_c G}{Y_b b_b t_b t_s} \right] \zeta = 0 \quad (31)$$

where  $G$  is the shear modulus of the bond layer material and  $\zeta$  is defined as the quantity  $(\varepsilon_c/\varepsilon_b - 1)$ . Making the substitution

$$\Gamma^2 = \frac{G}{Y_c t_c t_s} + \frac{3b_c G}{Y_b b_b t_b t_s} \quad (32)$$

leads to the governing equation for shear lag in the bond layer

$$\frac{\partial^2 \zeta}{\partial x^2} - \Gamma^2 \zeta = 0 \quad (33)$$

The general solution for this equation is

$$\zeta = A \cosh \Gamma x + B \sinh \Gamma x \quad (34)$$

with the boundary conditions

$$\text{at } x = 0 \quad \zeta = -1 \quad (35)$$

$$\text{at } x = l_c \quad \zeta = -1 \quad (36)$$

Solving these gives the complete solution as

$$\zeta = \frac{\cosh \Gamma l_c - 1}{\sinh \Gamma l_c} \sinh \Gamma x - \cosh \Gamma x \quad (37)$$

This variation is calculated both along the length and the width of the sensor, and the two effects are assumed to be independent, which means effects at the corners of the sensor are neglected. The function is plotted in Figure 6(a), along the length, for a PZT sensor of size  $6.67 \times 3.30 \times 0.25$  mm and in Figure 6(b), for a PVDF sensor of the same length and width, but of a thickness  $56 \mu\text{m}$ . The variations are plotted for different values of the bond layer thickness ratio,  $\Xi = t_s/t_c$  for both types of sensors. The values of  $\Xi$  are calculated by varying the bond layer thickness for a constant sensor thickness. The PVDF sensor shows a much lower shear lag loss than the PZT sensor for a given bond layer thickness ratio. This is due to the combined effect of lower sensor thickness and lower  $Y_c$  in the case of PVDF in Equation (32). As a result, the shear lag effect is almost negligible for a PVDF sensor.

To quantify the effect of the shear lag, effective dimensions are defined along the length and width of the sensor such that the effective sensor dimensions are subjected to a constant strain, which is the same as the assumed strain on the beam surface. By doing this, the sensor is assumed to be of new dimensions, smaller than the actual geometrical dimensions, over which  $Y = 1$  identically. The values of the effective length and width fractions,  $l_{eff}$  and  $b_{eff}$  respectively, can be obtained by integrating the area under the curves in Figure 6. For the sensor under discussion, which had a bond layer thickness of 0.028 mm ( $\Xi = 0.112$ ), the effective length fraction is 0.7646 and the effective width fraction is 0.4975. This means that only approximately 76% of the sensor length and 50% of the sensor width contribute to the total sensed strain. Because the whole geometric area of the sensor is no longer effective in sensing the beam surface strain, these correction factors must be inserted in the calibration equation Equation (14), which becomes

$$\varepsilon_1 = \frac{V_0}{K_b S_q^*} \quad (38)$$

where  $K_b$  is the correction factor to take care of shear lag effects in the bond layer. The value of  $K_b$  is independent of the material properties of the sensor, and is dependent only on its geometry. For both PZT and PVDF sensors,  $K_b$  is given by

$$K_b = l_{eff} b_{eff} \quad (39)$$

It should be noted here that for a PVDF sensor, the value of  $K_b$  is very close to unity [Figure 6(b)] and the shear lag effect can be neglected without significant error.

The final conversion relation from output voltage to longitudinal strain is

$$\varepsilon_1 = \frac{V_0}{K_p K_b S_q^*} \quad (40)$$

## RESULTS AND DISCUSSION

Experiments were performed on the beam bending setup as described above. For the sine sweeps, the beam was actuated from 5–500 Hz. A conventional 350  $\Omega$  foil strain gage was used, with a MicroMeasurements 2311 signal conditioning system. For the piezo sensor, a charge amplifier was built using high input impedance LF355 operational amplifiers, with  $R_F = 10$  M $\Omega$  and  $C_F = 10$  nF.

A major advantage of using piezoelectric sensors as opposed to conventional foil strain gages is their superior signal to noise ratio and high frequency noise rejection. Shown in Figure 7 is the impulse response from both the conventional foil strain gage and a PZT strain sensor. Both readings were taken simultaneously after the beam was impacted at the tip. Both the responses are unfiltered and show the actual recorded voltages from the signal conditioners. Note the large

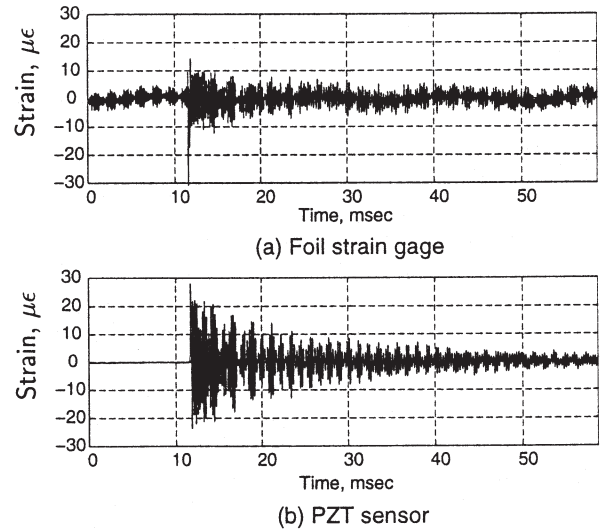


Figure 7. Foil strain gage and PZT sensor impulse response in the time domain.

amplitude background noise in the foil gage output, and the much higher signal to noise ratio of the PZT strain gage. The foil strain gage operates by sensing an imbalance in a Wheatstone bridge circuit, which is on the order of microvolts. Therefore, at low strain levels, the signal to noise ratio of foil strain gages is quite poor. The superior signal to noise ratio of piezoelectric sensors makes them much more attractive in situations where there is a low strain or high noise level. This can be seen more clearly in Figure 8 that shows the frequency response of the beam to a small impulse as recorded by a conventional foil strain gage and a PZT sensor. The spikes in the frequency response at 60 Hz, 120 Hz, 240 Hz, 360 Hz and 420 Hz are overtones of the AC power line frequency. Since the foil strain gage requires an excitation, its output can get contaminated with a component of the AC power line signal. PZT sensors are inherently free from

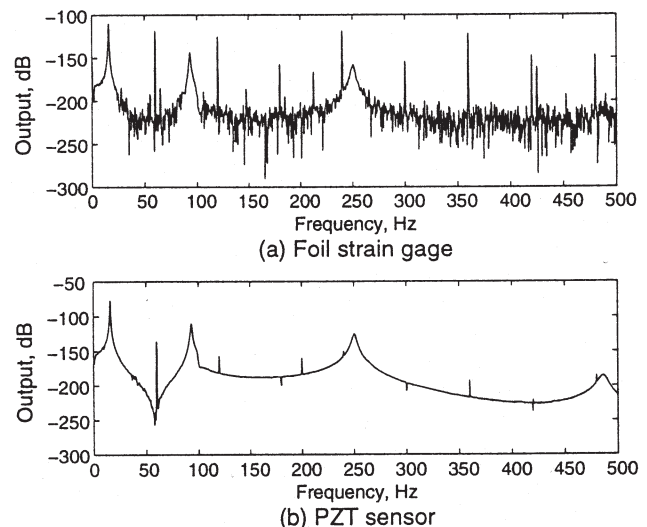
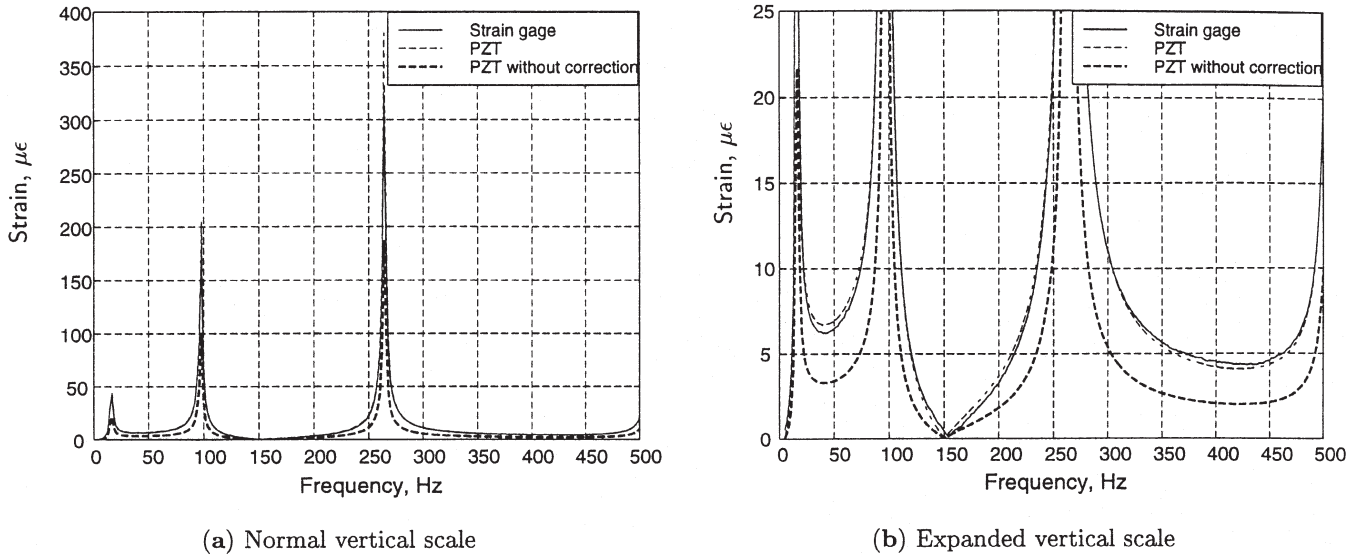


Figure 8. Foil strain gage and PZT sensor impulse response in the frequency domain.





**Figure 9.** Correlation of PZT sensor and foil strain gage with correction factor.

this contamination, however, the signal conditioning circuitry introduces some contamination into the PZT sensor output as well. It is worth mentioning here that the signal conditioning electronics associated with the foil strain gage is much more involved and bulky compared to that used in conjunction with the piezoelectric sensor.

The correlations between strain measured by a conventional strain gage and that measured by a PZT sensor are shown in Figures 9–11 for a sine sweep ranging from 5 Hz to 500 Hz. Figure 9 shows the correlation between the strain measurements from a strain gage and a PZT sensor after the appropriate correction factors are applied. The dimensions of the PZT sensor are  $3.5 \times 6.0 \times 0.23$  mm, and the value of  $C_F$  for this experiment is 1.1 nF. Also shown for comparison is the strain calculated from the PZT sensor readings without

application of the correction factors. It can be seen that the correction factors are very significant and after they are applied, there is very good agreement between the strains measured by the strain gage and the PZT sensor. Figure 10 shows a frequency sweep response at a very low excitation voltage, such that the strain response is only on the order of several microstrain. The sensor in this case is a PZT sensor of size  $6.9 \times 3.3 \times 0.23$  mm. Good correlation is observed over the whole frequency range, both in matching resonant frequencies as well as magnitude of the measured strain at off-resonant conditions. Hence, it can be concluded that the PZT sensors are capable of accurately measuring both low and high strain levels. It is to be noted that the strain gage is not able to accurately pick out the peak amplitudes at low strain levels. This clearly demonstrates the superiority of piezoelectric

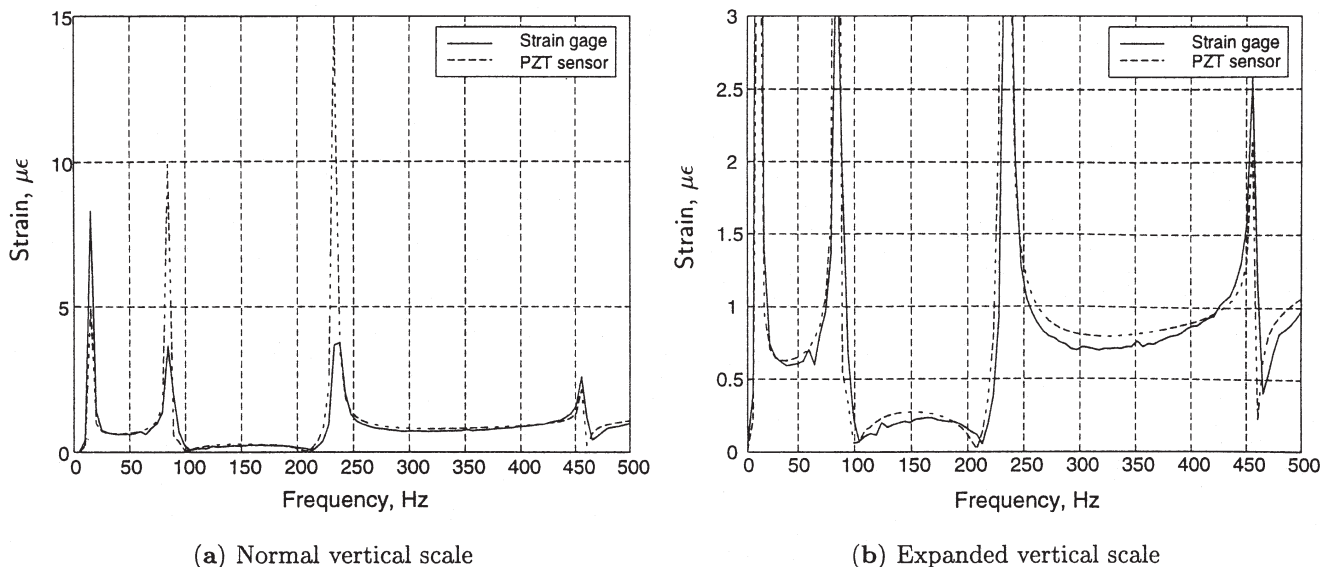
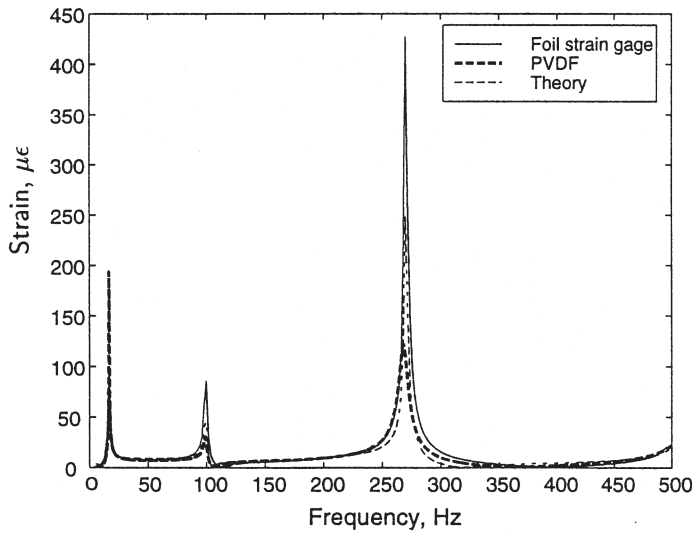
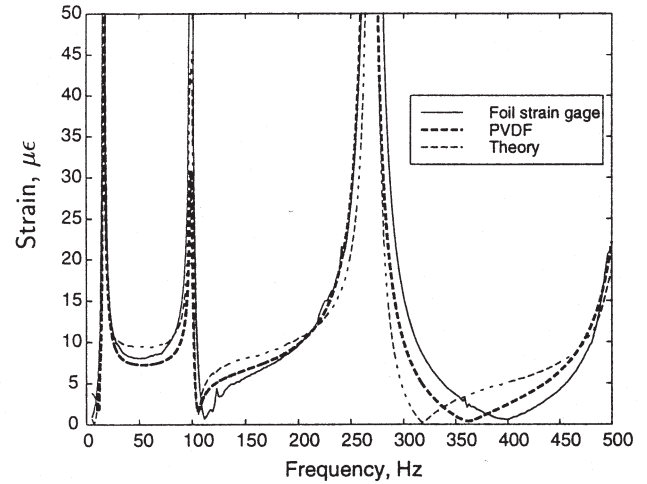


**Figure 10.** Correlation of PZT sensor and foil strain gage for response at low strain levels.



(a) Normal vertical scale



(b) Expanded vertical scale

Figure 11. Correlation of PVDF sensor and foil strain gage response.

sensors in such applications. The error between the foil strain gage and the PZT sensor is at most between 5–10% for off-peak conditions.

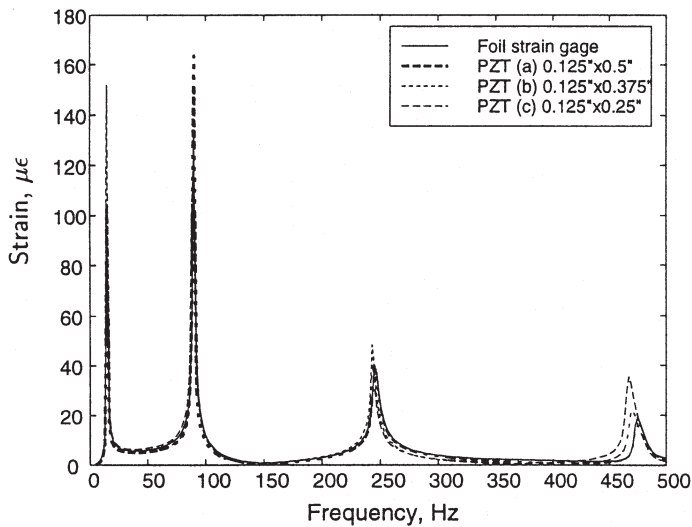
Figure 11 shows the results of replacing the PZT sensor with a PVDF sensor of size  $7.1 \times 3.6 \times 0.056$  mm, at higher strain levels. Again, good correlation is observed for lower frequencies, but at high frequencies, some discrepancy is apparent. Also plotted on the same figure is a prediction of the strain response at the sensor location calculated by an assumed modes method. The theoretical model uses a complex modulus with 3% structural damping. It can be seen that both sensors follow the same trend as that of the theoretical prediction. The discrepancy after the third resonant peak can be explained by a slight error in collocation of the foil strain

gage and the PVDF sensor. This difference in position gives rise to a shift in the zeros of the transfer function and the dynamics of these zeros affect the shape of the transfer function in this frequency range. The correlation in Figures 9 and 10 is better, however, since these tests were carried out on a different experimental beam setup.

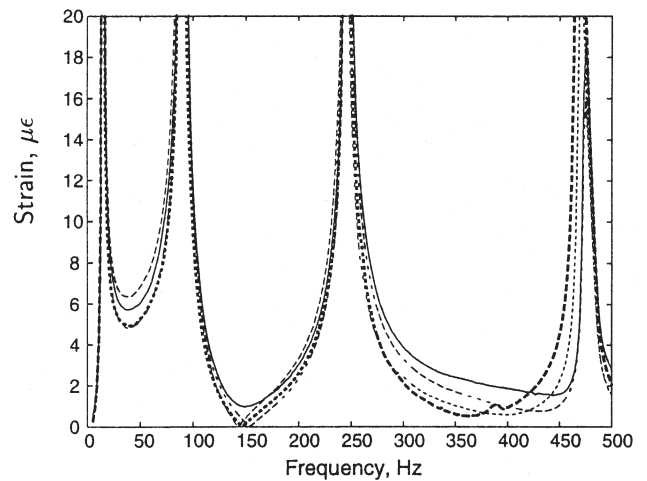
### General Operating Considerations

#### EFFECT OF SENSOR TRANSVERSE LENGTH

The size of the sensor is chosen on the basis of the desired gage length. The strain measurements from PZT sensors of three different sizes are shown in Figure 12. All three sensors have the same gage length of 0.125 inch, which is the same as



(a) Normal vertical scale



(b) Expanded vertical scale

Figure 12. Correlation of foil strain gage and PZT sensors of different sizes, keeping gage length constant.

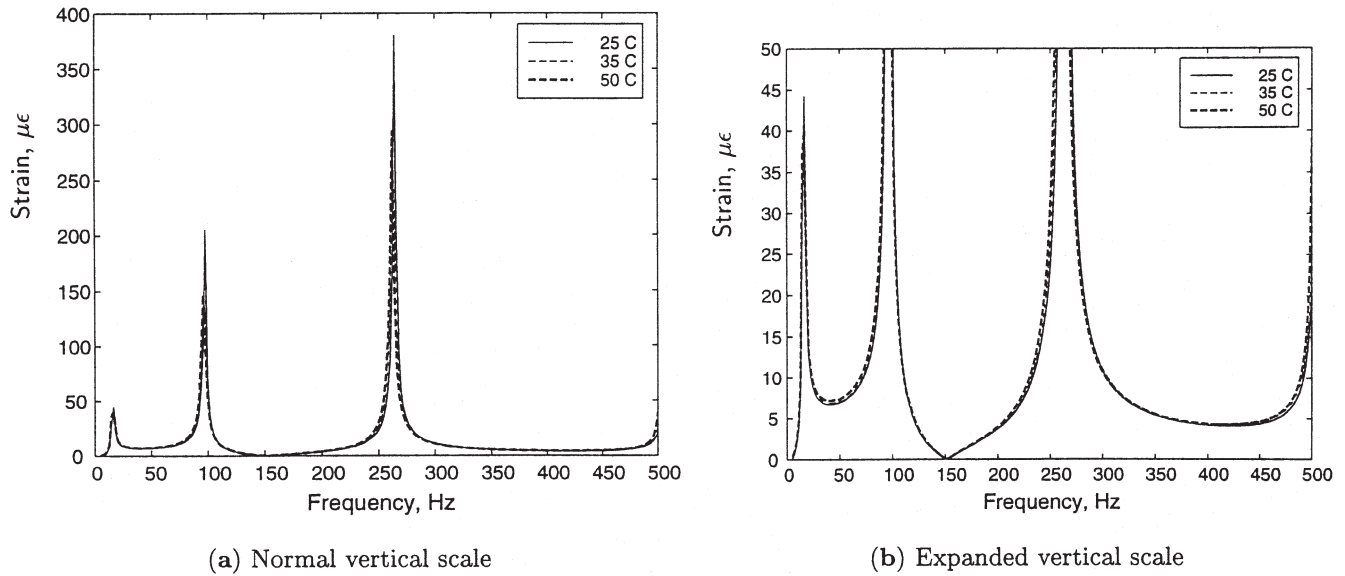


Figure 13. PZT sensor output variation with temperature.

the gage length of the foil strain gage also. The width of the sensors is varied and is 0.5 inch in case (a), 0.375 inch in case (b) and 0.25 inch in case (c). It can be seen that there is good correlation between strain gage and piezoelectric sensor irrespective of the sensor size. The primary effect of the sensor size can be seen from Equation (20). For a given sensor material, the output depends only on the area of the sensor,  $l_c b_c$ . A larger sensor would therefore produce a larger sensitivity. Assuming the sensing direction to be along  $l_c$ , for a constant gage length, the sensitivity can be increased by increasing the width of the sensor,  $b_c$ .

The secondary effect of sensor size can be seen from Equations (32) and (37). For a given sensor thickness  $t_c$  and bond thickness  $t_b$ , as the sensor dimensions increase, the shear lag losses decrease and the strain is transferred more efficiently from the surface of the structure to the sensor. The good correlation between PZT sensor strain measurements and conventional foil strain gages measurements irrespective of sensor size validates the theoretically derived shear lag correction factor.

Hence it can be concluded that the best strain sensitivity can be achieved by making the sensor area as large as possible, with the constraint of selecting an appropriate gage length for the application. It should also be pointed out that the sensor adds stiffness to the structure, and this additional stiffness increases with sensor size. This can be a significant factor in the case of PZT sensors, but will be normally negligible for PVDF sensors.

#### EFFECT OF TEMPERATURE ON SENSOR CHARACTERISTICS

The properties of all piezoelectric materials vary with temperature. In the case of piezoelectric ceramics, the variation with temperature is highly dependent on the material composition (Mattiati, 1971). Both the dielectric permittivity and

the piezoelectric coefficients vary with temperature. Since the charge amplifier effectively transfers the charge from the piezoelectric sensor onto a reference capacitor, the change in dielectric permittivity, and hence, the capacitance of the sensor with temperature has no effect on the sensor output. The only dependence of sensor output on temperature is due to the change in piezoelectric coefficients, as seen from Equation (20). As per the datasheets supplied by the manufacturer (Morgan Matroc, 1993), the magnitude of  $d_{31}$  increases by approximately 10% from room temperature (25°C) to 50°C. Tests were carried out in this temperature range by placing the entire experimental setup in an environmental chamber. The results are plotted in Figure 13, which shows a negligible change in sensor output without the use of any temperature correction factors. PVDF film exhibits pyroelectricity in addition to piezoelectricity, and hence, it has highly temperature dependent properties. PVDF film is sometimes used in temperature sensing. Care must be taken, therefore, to take measurements from PVDF sensors at known temperature conditions, and to use the appropriate values of the constants for calibration.

#### CONCLUSIONS

Piezoelectric materials show great promise in smart structural sensing applications. It has been found that the performance of piezoelectric sensors surpasses that of conventional foil type strain gages, with much less signal conditioning required, especially in applications involving low strain levels, and high noise levels. It is also possible to accurately calibrate these sensors. Using orthotropic materials like PVDF, it is possible to construct strain sensor configurations which enable the separation of different components in a general two-dimensional strain distribution.

However, it is not advisable to use these sensors to measure strain levels more than the order of 150 microstrain since nonlinearities and change in material properties, especially  $d_{31}$ , with stress will affect the accuracy of the calibration.

A very simple circuit was constructed to perform signal conditioning on the output of the piezoelectric sensor. The sensing system exhibits very good signal to noise output characteristics and its sensitivity can be adjusted by changing a component in the circuit, at the expense of frequency response. Good correlation with foil strain gage measurements has been demonstrated and the application of correction factors to the piezoelectric sensor output has been validated. It has been shown that for a constant gage length, sensitivity increases with increasing sensor area. Investigation of the effect of temperature conditions on the sensor response indicates that the output of the sensor needs no temperature correction over a moderate range of operating temperatures in spite of the fact that the piezoelectric coefficients are strongly temperature dependent. It can be concluded that piezoelectric strain sensors are a simple, easy to use and reliable alternative to conventional resistance based foil strain gages in a majority of smart structural applications.

## ACKNOWLEDGMENTS

This work was sponsored by the army research office under grant DAAH-04-96-10334 with Dr. Gary Anderson serving as technical monitor.

## REFERENCES

- IEEE Standard on Piezoelectricity*. 1987. ANSI/IEEE, Std. 176.
- Morgan Matric Inc. Piezoceramic Databook*. 1993. Morgan Matroc Inc., Electroceramics Division.
- Anderson, E. H. and N. W. Hagood. 1994. "Simultaneous Piezoelectric Sensing/Actuation: Analysis and Application to Controlled Structures," *Journal of Sound and Vibration*, 174(5):617–639.
- Brown, R. F. 1961. "Effect of Two-Dimensional Mechanical Stress on the Dielectric Properties of Ceramic Barium Titanate and Lead Zirconate Titanate," *Canadian Journal of Physics*, 39:741–753.
- Brown, R. F. and G. W. McMahon. 1962. "Material Constants of Ferroelectric Ceramics at High Pressure," *Canadian Journal of Physics*, 40:672–674.
- Chopra, I. 1996. "Review of Current Status of Smart Structures and Integrated Systems," *SPIE Smart Structures and Integrated Systems*, 2717:20–62.
- Crawley, E. F. and J. de Luis. 1987. "Use of Piezoelectric Actuators as Elements of Intelligent Structures," *AIAA Journal*, 25(10):1373–1385.
- Dally, J. W., W. F. Riley and K. G. McConnell. 1993. *Instrumentation for Engineering Measurements*. John Wiley and Sons, Inc.
- Esteban, J., F. Lalonde and C. A. Rogers. 1996. "Parametric Study on the Sensing Region of a Collocated PZT Actuator-Sensor," *Proceedings, 1996 SEM VIII International Congress on Experimental Mechanics*.
- Hanagud, S., M. W. Obal and A. J. Calise. 1992. "Optimal Vibration Control by the Use of Piezoelectric Sensors and Actuators," *Journal of Guidance, Control and Dynamics*, 15(5):1199–1206.
- Inman, D. J., J. J. Dosch and E. Garcia. 1992. "A Self-Sensing Piezoelectric Actuator for Collocated Control," *Journal of Intelligent Materials and Smart Structures*, 3:166–185.
- Kreuger, H. H. A. 1967. "Stress Sensitivity of Piezoelectric Ceramics: Pt. I. Sensitivity to Compressive Stress Parallel to the Polar Axis," *Journal of the Acoustical Society of America*, 42:636–645.
- Kreuger, H. H. A. 1968. "Stress Sensitivity of Piezoelectric Ceramics: Pt. III. Sensitivity to Compressive Stress Perpendicular to the Polar Axis," *Journal of the Acoustical Society of America*, 43:583–591.
- Lee, C. K. and T. O'Sullivan. 1991. "Piezoelectric Strain Rate Gages," *Journal of the Acoustical Society of America*, 90(2):945–953.
- Lee, C. K., T. C. O'Sullivan and W. W. Chiang. 1991. "Piezoelectric Strain Rate Sensor and Actuator Designs for Active Vibration Control," *Proceedings of the 32nd AIAA/ASME/ASCE/AHS/ASC Structures, Structural Dynamics and Materials Conference*, (4):2197–2207.
- Lin, M. W. and C. A. Rogers. 1993. "Modeling of the Actuation Mechanism in a Beam Structure with Induced Strain Actuators," AIAA-93-1715-CP.
- Lin, M. W. and C. A. Rogers. 1994. "Bonding Layer Effects on the Actuation Mechanism of an Induced Strain Actuator/Substructure System," *SPIE*, 2190:658–670.
- Mattiat, O. E., 1971. *Ultrasonic Transducer Materials*, Plenum Press, New York.
- Qui, J. and J. Tani. 1995. "Vibration Control of a Cylindrical Shell Using Distributed Piezoelectric Sensors and Actuators," *Journal of Intelligent Material Systems and Structures*, 6(4):474–481.
- Samuel, P. and D. Pines. 1997. "Health Monitoring/Damage Detection of a Rotorcraft Planetary Geartrain Using Piezoelectric Sensors," *Proceedings of SPIE's 4th Annual Symposium on Smart Structures and Materials*, San Diego, CA, 3041:44–53.
- Stout, D. F. 1976. *Handbook of Operational Amplifier Circuit Design*. McGraw-Hill Book Company.
- Varadan, V. K., X. Bao, C.-C. Sung and V. V. Varadan. 1989. "Vibration Control of Flexible Structures Using Piezoelectric Sensors and Actuators," *Journal of Wave-Material Interaction*, 4(1–3):65–81.